doi:10.1016/j.jmb.2009.11.005 J. Mol. Biol. (2010) 396, 47–59

JMB

Available online at www.sciencedirect.com

ScienceDirect

ELSEVIER

Structural Bases for Stability–Function Tradeoffs in Antibiotic Resistance

Veena L. Thomas[1,2], Andrea C. McReynolds[2] and Brian K. Shoichet[2]*

[1]*Graduate Program in Pharmaceutical Sciences and Pharmacogenomics, University of California San Francisco, San Francisco, CA 94158-2518, USA*

[2]*Department of Pharmaceutical Chemistry, University of California San Francisco, Room 508D, Byers Hall, 1700 4th Street, San Francisco, CA 94158-2550, USA*

Received 9 September 2009; received in revised form 2 November 2009; accepted 4 November 2009
Available online 10 November 2009

Preorganization of enzyme active sites for substrate recognition typically comes at a cost to the stability of the folded form of the protein; consequently, enzymes can be dramatically stabilized by substitutions that attenuate the size and preorganization "strain" of the active site. How this stability–activity tradeoff constrains enzyme evolution has remained less certain, and it is unclear whether one should expect major stability insults as enzymes mutate towards new activities or how these new activities manifest structurally. These questions are both germane and easy to study in β-lactamases, which are evolving on the timescale of years to confer resistance to an ever-broader spectrum of β-lactam antibiotics. To explore whether stability is a substantial constraint on this antibiotic resistance evolution, we investigated extended-spectrum mutants of class C β-lactamases, which had evolved new activity *versus* third-generation cephalosporins. Five mutant enzymes had between 100-fold and 200-fold increased activity against the antibiotic cefotaxime in enzyme assays, and the mutant enzymes all lost thermodynamic stability (from 1.7 kcal mol^{-1} to 4.1 kcal mol^{-1}), consistent with the stability–function hypothesis. Intriguingly, several of the substitutions were 10–20 Å from the catalytic serine; the question of how they conferred extended-spectrum activity arose. Eight structures, including complexes with inhibitors and extended-spectrum antibiotics, were determined by X-ray crystallography. Distinct mechanisms of action, including changes in the flexibility and ground-state structures of the enzyme, are revealed for each mutant. These results explain the structural bases for the antibiotic resistance conferred by these substitutions and their corresponding decrease in protein stability, which will constrain the evolution of new antibiotic resistance.

Keywords: protein stability; AmpC β-lactamase; antibiotic resistance; evolution; action at a distance

Edited by G. Schulz

Introduction

In engineering a protein for stability, among the surest places to make substitutions is the active site. This will appear paradoxical to many because these active-site substitutions typically reduce the activity of the mutant protein, and an inactive but stable mutant enzyme is rarely sought. Still, this trading of activity for stability illustrates a point: active sites are typically those regions in proteins that manifest the most internal strain. In active sites, polar groups are sequestered from water,[1,2] like-charged residues cluster together, residues adopt strained conformations,[3] and hydrophobic patches are exposed.[4] As Warshel,[1]Warshel *et al.*,[2] Richards,[5] and Williams[6] have suggested, this strain preorganizes the active site for ligand recognition and catalysis, and is paid for at the time of folding by the net overall stability conferred by the rest of the protein. The conversion of active-site "strain" into increased stability was first tested in barnase,[7] barstar,[8] T4 lysozyme,[9] and AmpC β-lactamase,[10] where point

*Corresponding author. E-mail address: shoichet@cgl.ucsf.edu.

Present address: A. C. McReynolds, Room ND7.202, UT Southwestern Medical Center at Dallas, 6001 Forest Park Road, Dallas, TX 75390-9041, USA.

Abbreviations used: TEM, tumor endothelial marker; ESBL, extended-spectrum β-lactamase; WT, wild type; BZB, benzo(*b*)thiophene-2-boronic acid; HIV, human immunodeficiency virus; PDB, Protein Data Bank.

substitutions increased enzyme stability by up to 4 kcal mol^{-1} (or 30% of the net overall stability). Subsequent studies are consistent with the idea that residues important for function may be suboptimal for stability,[11–16] and that enzymes may be substantially stabilized by active-site substitutions that attenuate activity.[17–19]

If there is, by now, much support for the idea that enzymes can be stabilized by active-site substitutions, the "stability–function hypothesis"[9] (the logical corollary) that they will often lose stability as they gain activity has been more controversial. In a study of the antibiotic resistance enzyme tumor endothelial marker (TEM)-1 β-lactamase, we found that clinically selected gain-of-activity mutants lost stability to the point where a secondary site substitution (far from the active site) that restored stability and allowed further destabilizing gain-of-resistance mutants to evolve occurred.[20–22] Subsequently, Weinreich *et al.* showed that the pathways to stable and active TEM mutants were epistatic and cooperative, consistent with a stability constraint on enzyme evolution.[23] On the other hand, Giver *et al.* has argued that the apparent stability–activity tradeoffs, simply reflecting differing constraints, may be unrelated: enzymes being evolved for activity will give up stability because it is not being as strongly selected, whereas an enzyme being evolved for stability may give up activity for the same reason.[24] Although there is agreement that enzymes that are stabilized[25,26]—or buffered against unfolding by chaperones[27]—are more evolvable, consensus around a correlation between stability and activity in enzyme evolution has not emerged.

These two views may be reconcilable. At its heart, the stability–activity tradeoff hypothesis is about competing physical interactions in the active site. For those enzymes that evolve new activity by increasing active-site preorganization, for instance by increasing active-site size to accommodate larger substrates, tradeoffs in stability seem physically necessary. However, not all gain-of-function mutants fit this pattern. For instance, a thermophilic enzyme selected for activity may give up its stability simply because this is not being selected for.[24] Similarly, one can imagine a protein that evolves to recognize a simpler substrate—one that requires less preorganization than its ancestral substrate; in this case, the mutant enzyme might well gain *both* activity and stability relative to the ancestral protein. But for situations where a new active site is being

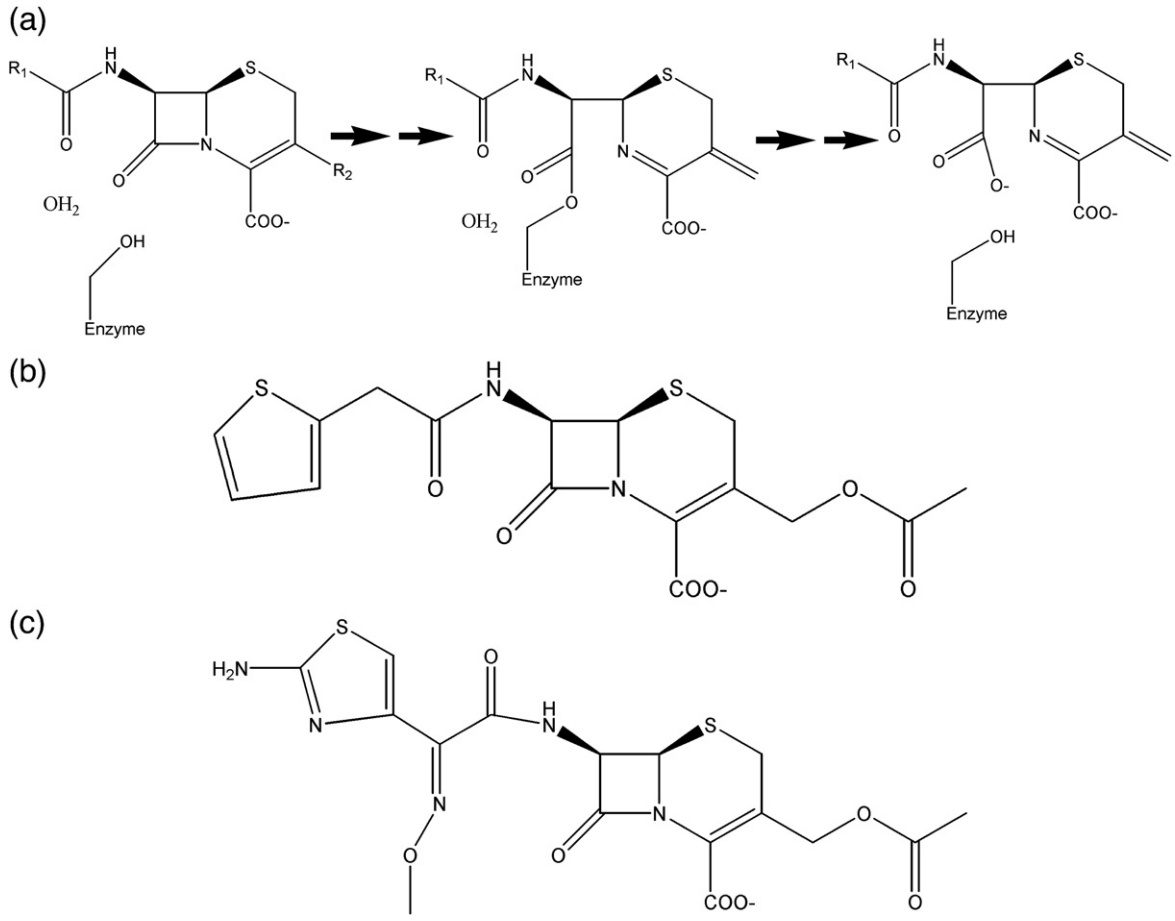

Fig. 1. β-Lactamase reaction mechanism and representative antibiotic substrates. (a) Reaction mechanism of AmpC β-lactamase. (b) The first-generation cephalosporin antibiotic cephalothin. (c) The third-generation cephalosporin antibiotic cefotaxime.

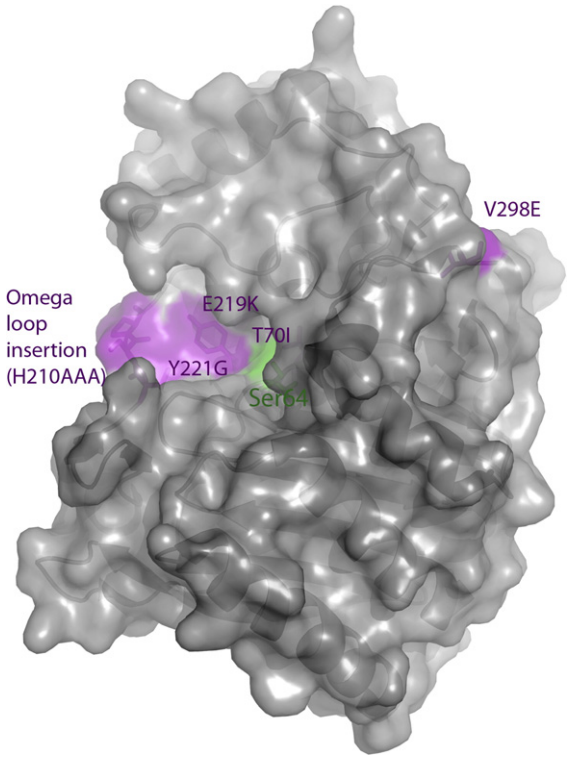

Fig. 2. ESBL substitutions under investigation in AmpC β-lactamase (in purple). The catalytic serine is shown in green.

created, or an established one is being enlarged or further preorganized, then by physical necessity we expect stability (unless otherwise compensated for) to be sacrificed.

The experimental support for stability–activity tradeoffs in enzyme evolution rests largely on a study of TEM-1 β-lactamase,[20] and it seemed worthwhile to explore generality in another enzyme. We turned to the class C β-lactamase AmpC, which, although also a β-lactamase, diverged from class A enzymes hundreds of million years ago, with the two families sharing no measurable sequence identity and differing from each other in size, domain organization, and mechanistic details.[28–30] AmpC family enzymes confer resistance to β-lactam antibiotics (Fig. 1a and b) and are key resistance determinants in hospital-acquired pathogens, especially against cephalosporin β-lactams. "β-Lactamase-stable" third-generation cephalosporins, such as ceftazidime and cefotaxime (Fig. 1c), were introduced in the early 1980s to overcome resistance conferred largely by class A β-lactamases, but they are also poor substrates for AmpC, whose active site is essentially too small to accommodate them. Thus, when these large third-generation cephalosporins form covalent adducts with AmpC, they are forced into a conformation that is incompetent for catalysis due to steric clashes between their bulky R1 side chain and residues Val211 and Tyr221.[31] "Extended-spectrum" β-lactamase (ESBL) mutants with increased hydrolytic activity against third-generation cephalosporins have subsequently appeared both in the clinic[32–35] and as a product of *in vitro* evolution and mutagenesis.[36–39] Because these mutant enzymes were evolving to recognize substrates that were too large for the native active site, but in which catalysis would retain the same location and same chemistry, they seemed like good templates to explore for stability–activity tradeoffs.

Here we investigate five extended-spectrum mutants of AmpC (Fig. 2) by asking the following questions: Are these mutants in fact better enzymes for the third-generation cephalosporins and are not simply, for instance, overexpressed in resistant cells? Does any gain of activity come with a concomitant loss of stability? Since stability–activity tradeoffs are formulated as biophysical compensations, is stability change thermodynamic, as reflected by reversible two-state thermal denaturation? The stability–function hypothesis applies to improved substrate complementarity arising from the introduction of structural defects or increasing residue preorganization; to investigate this, we determine X-ray crystal structures of the five mutant enzymes. These structures also reveal how substitutions that are distant from the active site, as occur with resistance mutations in many enzymes,[40–42] can transduce their perturbations to the active site and thereby increase catalytic activity.

Results

Function–stability tradeoffs

Five ESBL mutants—V298E,[39] "Ω-loop insertion" (H210AAA),[32–34] T70I,[36] Y221G,[37] and E219K[35,38]—were made by site-directed mutagenesis and purified to apparent homogeneity, and the kinetic constants

Table 1. Kinetic and thermodynamic parameters of AmpC ESBL mutants

Mutation	C_α–C_α distance to Ser64 (Å)	Melting temperature (T_m)	ΔT_m (°C)	$\Delta\Delta H$ (kcal mol^{-1})	$\Delta\Delta G$ (kcal mol^{-1})	Cephalothin		Cefotaxime	
						K_m (μM)	k_{cat} (s^{-1})	K_m (μM)	k_{cat} (s^{-1})
WT	NA	54.6	—	182	—	27	420	0.8	0.0448
T70I	10.0	51.5	−3.1	142	−1.74	53	53.9	295	9.2
V298E	21.0	47.2	−7.4	102	−4.14	32	90.6	79	4.4
E219K	9.3	48.6	−6.0	180	−3.36	24	84.6	77	6.9
Y221G	4.6	50.8	−3.8	199	−2.13	99	4.2	337	8.0
Ω-loop insertion (residue 210)	14.5	51.3	−3.3	183	−1.85	23	134	53	8.7

k_{cat} and K_m against the first-generation cephalosporin cephalothin and the third-generation cefotaxime were determined. All of the ESBLs had increased activity against cefotaxime relative to wild-type (WT) AmpC, as measured by k_{cat}, typically by 100-fold to 200-fold (Table 1, Fig. 3a). Normally, one would use k_{cat}/K_m to compare the relative activities of the WT and mutant enzymes; however, for class C β-lactamases, this value is misleading. Since the acylation rate constant (k_2) for β-lactams is fast on the scale of the pre-covalent disassociation constant (k_{-1}), the K_m values for these enzymes do not reflect a disassociation constant, but rather the deacylation rate constant ($k_3 = k_{cat}$) divided by the acylation rate constant (k_2). Thus, k_{cat}/K_m collapses to simply k_2, making what would ordinarily be considered the "specificity constant" misleading.[43] Because k_{cat} is slow for the WT enzyme ($k_{cat} = 0.0448\ s^{-1}$ for cefotaxime in WT AmpC),[44] K_m values are typically too low to be measured, and IC_{50} is typically used as proxy for K_m.[44,45] For these enzymes, k_{cat} comparisons are more informative. This can be illustrated by an example. For WT AmpC, the k_{cat} for cefotaxime is $0.0448\ s^{-1}$ and the IC_{50}-derived K_m is 0.8 μM, resulting in a k_{cat}/K_m of $5.6 \times 10^4\ M^{-1}\ s^{-1}$. For V298E, k_{cat} is $4.4\ s^{-1}$ (Table 1) and K_m is 79 μM, resulting in the same k_{cat}/K_m value as the WT enzyme. However, 50 nM V298 will hydrolyze 50 μM ceftazidime (a physiologically relevant concentration) in minutes, while WT AmpC at the same concentration would take close to half a day. This gain in new activity against cefotaxime was accompanied by a corresponding loss of native activity against cephalothin, typically from 3-fold to 8-fold, but as high as 100-fold in the case of Y221G (Table 1, Fig. 3a).

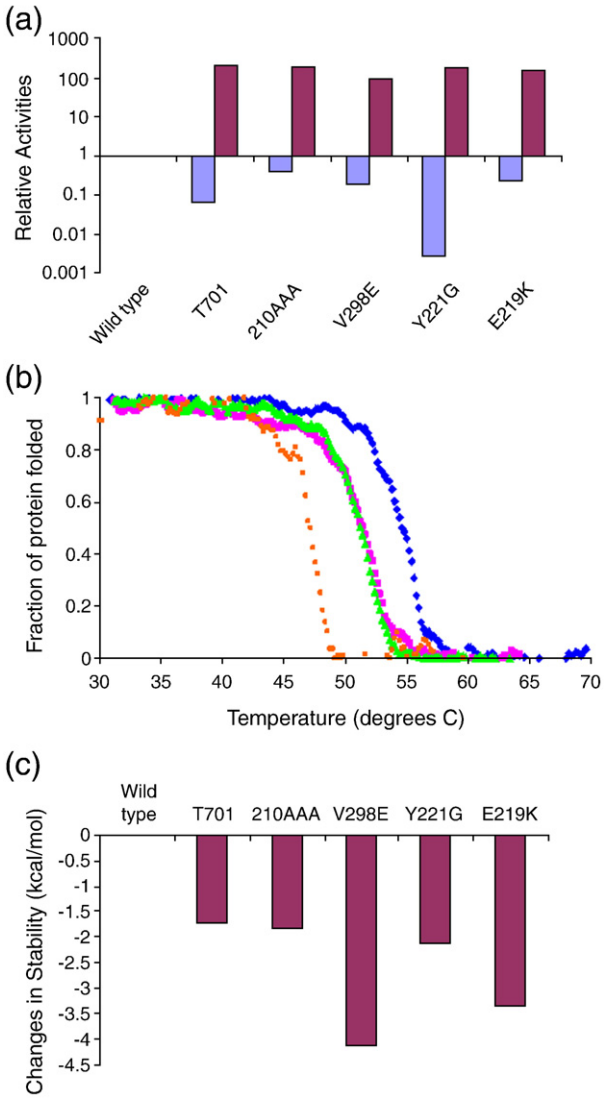

Fig. 3. Relative enzyme activities and thermodynamic stabilities of AmpC ESBL mutants. (a) Relative activities of AmpC ESBLs against the first-generation cephalosporin cephalothin (blue) and the third-generation cephalosporin cefotaxime (purple). (b) Characteristic thermal denaturation curves of selected AmpC ESBL mutants (V298E, orange; Ω-loop insertion, green; T70I, magenta) relative to the WT enzyme (blue). (c) The differential stabilities of AmpC ESBL mutants relative to those of WT AmpC.

The stability of the ESBL mutants was determined by thermal denaturation, monitored by far-UV circular dichroism (CD). In determining the thermodynamic stability of these mutant enzymes, it is necessary to demonstrate their reversibility and two-state behavior upon thermal unfolding. Extensive previous work suggests that WT and mutant AmpC enzymes denature reversibly and in a two-state manner:[46] they reversibly denature both by rapid cooling and by slow reannealing from the unfolded state in temperature melts. T_m and ΔH_u are very similar when measured by far-UV CD and near-UV CD; by fluorescence, T_m is unaffected by ramp rates between 0.5 °C min^{-1} and 2 °C min^{-1}, and the transition itself is well fitted by a two-state model.[46] The thermal denaturation of each extended-spectrum AmpC mutant monitored by far-UV CD was also consistent with a reversible two-state model. Melting curves showed clear two-state behavior, with a clear and sharp transition at the melting temperature (Fig. 3b). Denaturation was reversible, ranging from 90% to 100% of the CD signal regained after quick cooling of the denatured enzymes. The thermal denaturation of a representative mutant, Y221G, monitored by fluorescence emission, also showed a sharp transition with the same T_m of 50.8 °C as when monitored by far-UV CD (Supplementary Material, Fig. S1a). A second ESBL mutant, the Ω-loop insertion, also showed a sharp transition with a T_m of 52.1 °C (compared to a T_m of 51.3 °C by CD) when monitored by far-UV CD (Supplementary Material, Fig. S1b). We therefore assume that these mutants, like the WT enzyme, denature in a reasonable approximation to a reversible two-state behavior, allowing us to determine the true thermodynamic differences in enzyme stability relative to the WT enzyme.

The thermodynamic stability of all five ESBLs was decreased relative to the WT enzyme (Table 1, Fig. 3c). The melting temperatures of these mutant enzymes diminished by between 3.1 °C and 7.4 °C, corresponding to a 1.7–4.1 kcal mol^{-1}decrease in stability—a substantial change in stability for single

Table 2. Crystallographic statistics

Protein	V298E	Ω-Loop insertion	T70I/BZB	Y221G	Y221G/ cefotaxime	E219K	E219K/BZB
Data collection							
Space group	$P2_1$	*C*2	*C*2	*C*2	*C*2	*C*2	*C*2
Cell dimensions							
a, *b*, *c* (Å)	81.271	117.582	114.162	117.717	117.80	118.247	117.06
	75.852	77.926	77.361	76.789	77.58	76.876	77.41
	84.086	98.050	91.747	98.693	98.89	116.492	97.24
α, β, γ (°)	90.00	90.00	90.00	90.00	90.00	90.00	90.0
	115.96	115.96	122.12	116.62	118.60	130.89	115.58
	90.00	90.00	90.00	90.00	90.00	90.00	90.0
Resolution (Å)	30.0–2.64 (2.70–2.64)*)[a]	30.0–1.64 (1.68–1.64)	30.0–2.64 (2.70–2.64)	30.0–1.90 (1.95–1.90)	60.02–2.30 (2.42–2.30)	30.0–1.84 (1.88–1.84)	30.0–1.63 (1.67–1.63)
R_{merge} (%)	8.9	6.1	7.1	6.8	10.6	9.4	6.1
$I/\sigma I$	8.0 (2.0)	8.7 (2.3)	7.8 (2.1)	7.7 (2.1)	4.5 (2.3)	5.1 (2.2)	8.4 (2.0)
Completeness (%)	100.0 (100.0)	100.0 (99.9)	98.4 (97.0)	99.9 (99.9)	96.9 (96.2)	94.0 (93.2)	99.9 (100.0)
Refinement							
Number of reflections	28,233 (2080)	92,466 (6818)	34,977 (2548)	58,776 (4295)	32,017 (2363)	60,887 (4418)	92,583 (4868)
R_{work}/R_{free} (%)	18.4/23.4	17.0/19.7	19.6/24.7	15.7/19.7	19.6/24.8	17.4/21.7	17.6/20.8
Number of atoms							
Protein	5577	6297	5316	5541	5610	5549	5565
Ligand/ion	6	0	12	74	28	10	44
Water	119	278	249	577	187	737	865
B-factors (Å^2)							
Protein	24.8	15.3	27.90	17.36	29.96	18.49	16.48
Ligand/ion	52.8	44.3	32.75	42.7	45.7	39.10	23.93
Water	37.358	36.9	30.81	30.71	30.79	27.65	28.41
RMSD							
Bond lengths (Å)	0.013	0.016	0.011	0.015	0.013	0.015	0.010
Bond angles (°)	1.494	1.486	1.414	1.460	1.437	1.465	1.383

[a] Values in parenthesis represent the highest-resolution shells.

substitutions, particularly since the overall stability of the WT enzyme is only 14 kcal mol^{-1}.[46]

V298E apo structure

The structure of the V298E mutant enzyme was determined by X-ray crystallography to 2.64 Å resolution (R_{work}=18.4%, R_{free}=23.4%; Table 2). A well-defined $2F_o-F_c$ electron density at a contour level of 1σ was seen for most residues in the structure, with the exception of residues 285–296 (Fig. 4; Supplementary Material, Fig. S2). The resulting structure reveals a "domino effect" of structural changes, starting at the point of substitution and transmitting to the active site 20 Å away (Fig. 4). Val298 is found in a mini-hydrophobic core of the WT enzyme; when substituted to a glutamate, Glu298 moves to enable its interaction with solvent, opening up a cavity in the hydrophobic core (Fig. 4). The side chain of Trp260 adopts a conformation where it can fill this cavity. The new position of Glu298 clashes with the position of Pro297 in the WT

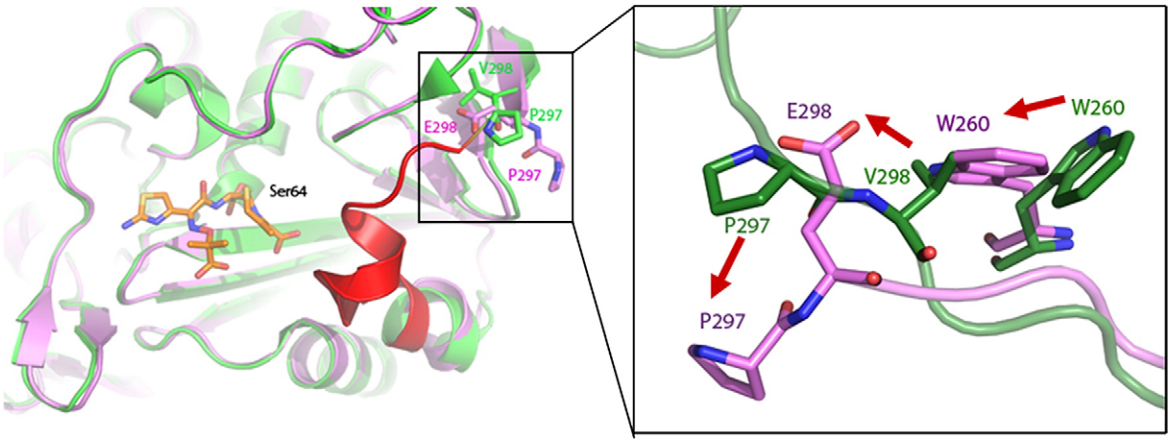

Fig. 4. The X-ray crystal structure of V298E to 2.6 Å resolution, showing an overview of changes in the V298E mutant (purple) compared to the WT protein (green). Density is lost for the region of the loop shown in red, presumed to have flipped out. Structural changes are shown at the point of mutation (inset), with the mutant protein (purple) overlaid on the WT protein (green).

enzyme; to avoid this clash, Pro297 swings out. This residue is on one end of a loop forming one wall of the active site; when it adopts this new conformation, it presumably takes the rest of the loop with it, as density is lost for residues 285–296 in this structure (Fig. 4). The positions of key active-site residues resemble that of the WT AmpC structure, with the exception of Tyr150, which adopts a new conformation where it hydrogen bonds with Lys315. As an aside, we observed strong positive F_o-F_c density connecting atom $C_{\varepsilon 2}$ of Tyr150 and atom N_ζ of Lys67. We also observed this feature in the Ω-loop insertion apo crystal structure (see the text below), and a similar feature was observed in the crystal structure of the Ω-loop insertion GC1 from *Enterobacter cloacae*.[32] In the GC1 structure, this feature was left unmodeled, but was attributed to a reaction with sodium azide present in the crystallographic buffer; we have also chosen not to model this feature.

Ω-Loop insertion apo structure

The three-residue Ω-loop insertion was originally identified as a clinical isolate in the class C P99 β-lactamase from *E. cloacae* and was subsequently characterized.[32–34,47] In addition, two structures of this extended-spectrum class C β-lactamase were determined: in apo form[32] and in complex with a cefotaxime phosphonate transition-state analog.[33] Inspired by this work, we decided to study the thermodynamic implications of this substitution and, for consistency, made the analogous mutation in AmpC. Since it was determined that the length—not the identity—of the insertion was crucial in imparting catalytic activity, and that an insertion of three alanines had comparable extended-spectrum activity,[34,47] we used an insertion of three alanine residues after His210 to represent the Ω-loop insertion. The structure of the apo Ω-loop insertion structure was determined to 1.64 Å resolution by X-ray crystallography ($R_{work}=17.0\%$, $R_{free}=19.7\%$; Table 2). Overall, the Ω-loop insertion structure resembles the WT structure; the RMSD for C_α atoms is 0.16 Å. However, in the region of the Ω-loop, at the terminus of the active site, the changes are substantial. In the mutant, the insertion causes the Ω-loop to adopt a new conformation (Fig. 5a and b); the C_α of Pro216 has moved by 8.9 Å, relative to the WT Pro213. Similarly, Val211 has moved by 8.5 Å and has, in essence, been replaced by Ala211. In addition, Tyr221 OH has moved by 1.1 Å, and Tyr221 C_δ, the atom thought to sterically clash with a catalytically competent conformation of third-generation cephalosporins, has shifted by 0.6 Å. Well-defined $2F_o-F_c$ electron density at a contour level of 1σ was seen for most residues in the structure, with the exception of residues 287–293 in the A monomer (the positions cannot be resolved for residues 285–290 in the A monomer of the WT enzyme). The key active-site residues resemble that of the WT AmpC structure, with the exception of Tyr150, which adopts a new conformation where it hydrogen bonds with Lys315.

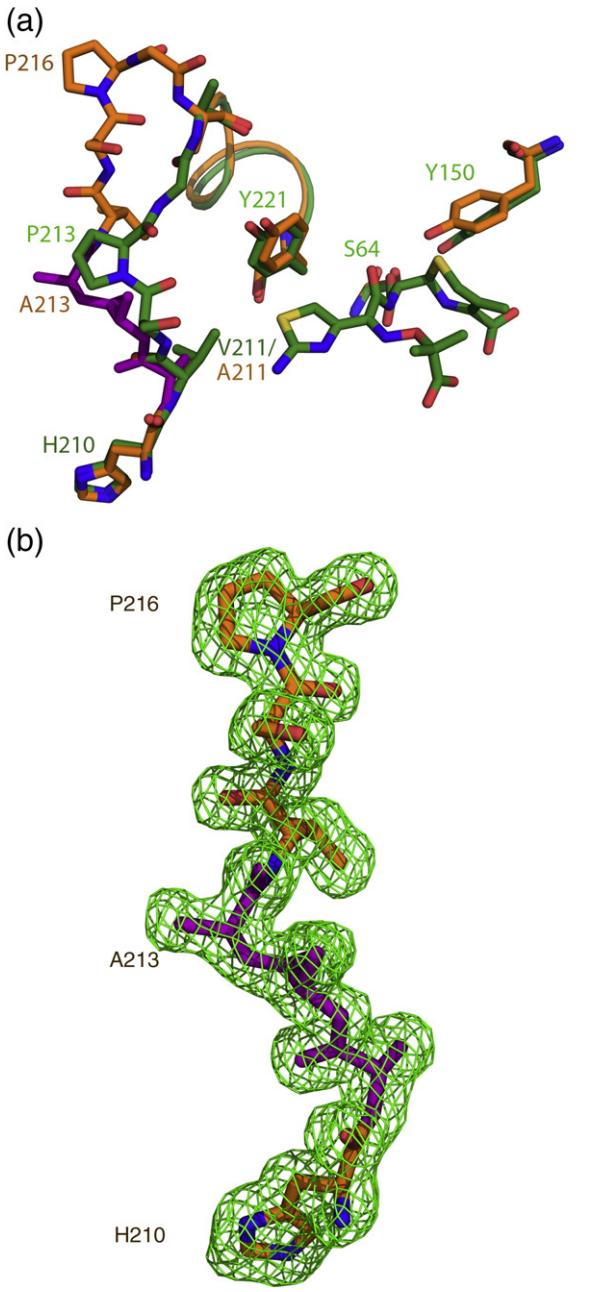

Fig. 5. The X-ray structure of the "Ω-loop insertion" mutant (H210AAA) to 1.6 Å resolution. (a) The Ω-loop insertion structure (orange; three-alanine insertion in purple) overlaid on the WT protein (green). (b) F_o-F_c omit density for residues 210–216 shown at 3σ.

T70I apo and holo structures

T70I was crystallized out of a buffer containing the transition-state analog benzo(*b*)thiophene-2-boronic acid (BZB; $K_i=27$ nM) against the wild-type enzyme[48] after repeated attempts to grow apo T70I crystals failed. The structure of T70I was determined by X-ray crystallography to 2.14 Å resolution ($R_{work}=19.6\%$,

R_{free} = 24.7%; Table 2). Like all AmpC structures, the protein, although functionally a monomer, crystallized with two monomers in the asymmetric unit. Surprisingly, one monomer was an apo structure, and the other had the transition-state analog bound to the active site; each monomer adopted a different conformation (Fig. 6). In the apo monomer, no electron density was seen for residues 193–221, comprising the Ω-loop of the enzyme. In addition, the β-turn from residues 318–322 has flipped into the active site, disorganizing the region around the oxyanion hole formed by the backbone nitrogens of the catalytic Ser64 and Ala318 (Fig. 6a). The active site of the T70I/BZB structure (Fig. 6b) conversely resembles that of the WT AmpC/BZB structure.[48] In addition, unlike in the apo structure, strong electron

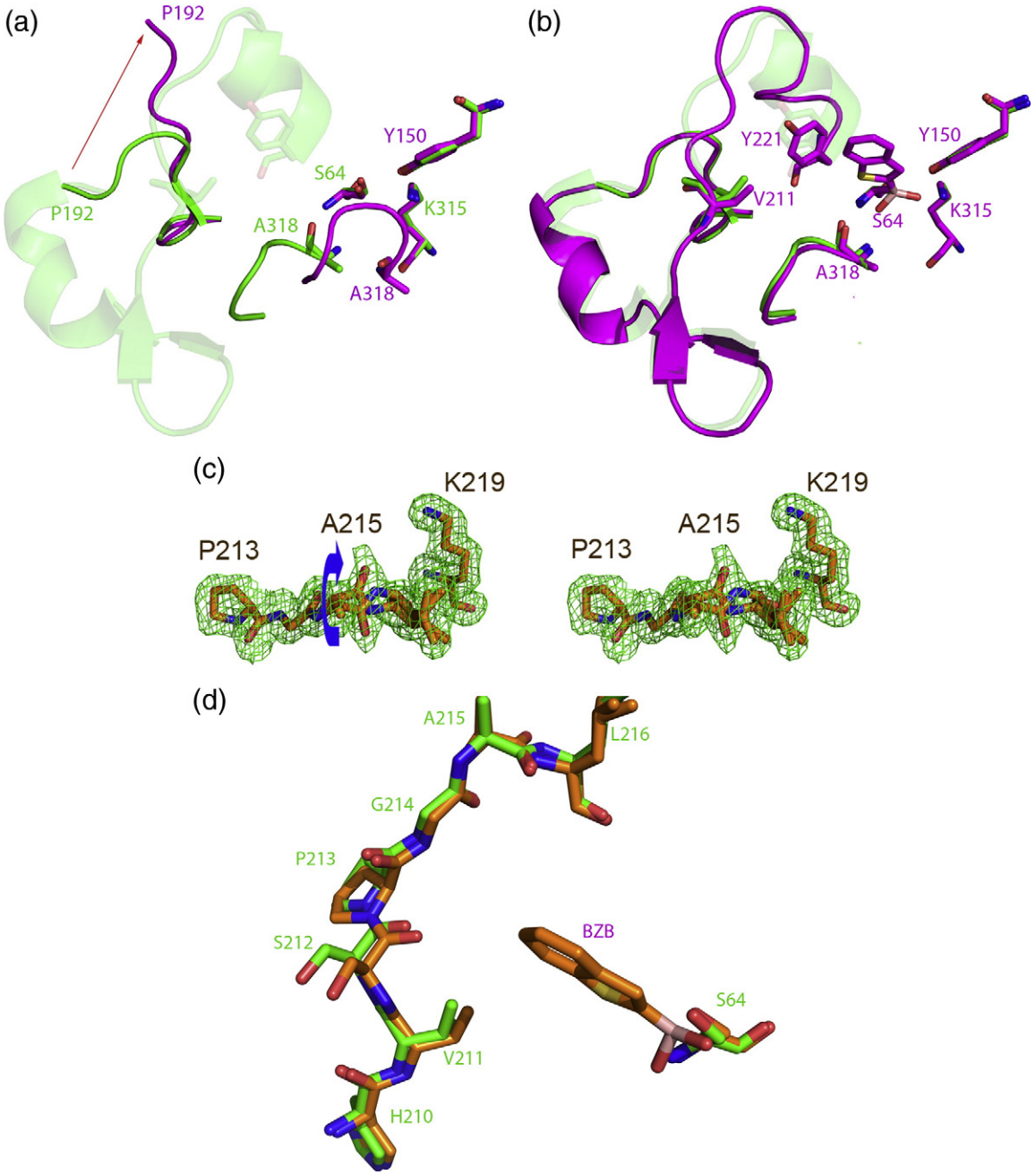

Fig. 6. Flexibility induced in extended-spectrum mutants T70I and E219K. (a) The T70I apo structure (purple) overlaid on the WT structure (green). Density is lost from residues 193–221 in the Ω-loop (transparent green) in the T70I structure. (b) The T70I/BZB structure (purple) overlaid on the WT structure (green). Residues 193–221, lost in the T70I structure but present in the T70I/BZB structure, are shown in cartoon. (c) Stereo view of the X-ray crystal structure of E219K/BZB to 1.63 Å resolution. $F_o - F_c$ omit density is shown at 3σ. Arrow highlights the two conformations of residues 215–216, distinguished by a peptide flip. (d) The Ω-loop and active site of E219K/BZB (orange) overlaid with that of the WT AmpC structure (green) showing conformational differences in the 211–213 region. The position of BZB is shown in the active site.

density is seen for residues 193–221 at 1σ, allowing the positions of these residues to be determined (Fig. 6b). This region now adopts a slightly different conformation than it does in the WT AmpC structure, predominately in the region from residues 211–216 (Fig. 6b); it enlarges the active site in some regions, although it is closer to the active site in others.

E219K apo and holo structures

The E219K apo structure was determined to 1.84 Å resolution (R_{work} = 17.4%, R_{free} = 21.7%; Table 2), and its complex with the transition-state analog inhibitor BZB was determined to 1.63 Å resolution (R_{work} = 17.6%, R_{free} = 20.8%; Table 2). After an initial round of refinement with the WT enzyme as model, a negative $F_o - F_c$ density was seen at 3σ for Glu219, with a nearby positive $F_o - F_c$ density at 3σ resembling a lysine. This residue was computationally mutated to a lysine, and the structure was further refined. $2F_o - F_c$ density was unambiguous at the point of substitution for Lys219 in both final structures, verifying the substitution (Supplementary Material, Fig. S3a). The position of this side chain in both structures resembles that of Glu219 in the WT structure, pointing to the solvent (Supplementary Material, Fig. S3b). In the WT enzyme, the side chain of Glu219 hydrogen bonds to its own backbone amide nitrogen. Substitution of this residue to a lysine removes this interaction, and the K219 backbone nitrogen now hydrogen bonds with the backbone carbonyl of Leu216, which has moved closer to it (Fig. 6c). This, in turn, affects the conformation of residues 215–216 in the E219K/BZB structure. In the WT structure, the backbone nitrogen of Asp217 hydrogen bonds with the backbone carbonyl of Ala215. With the carbonyl of Leu216 now engaged with the backbone nitrogen of Lys219, residues 215–216 now adopt two conformations, with the peptide backbone flipped relative to each other (Fig. 6c). Also, residues 211–213, also in the Ω-loop, now adopt a conformation different from that in the WT AmpC structure (Fig. 6d).

Y221G apo structure

The Y221G apo structure was determined to 1.90 Å resolution (R_{work} = 15.7%, R_{free} = 19.7%; Table 2). Few structural changes are seen in Y221G compared to the WT AmpC structure. Substitution

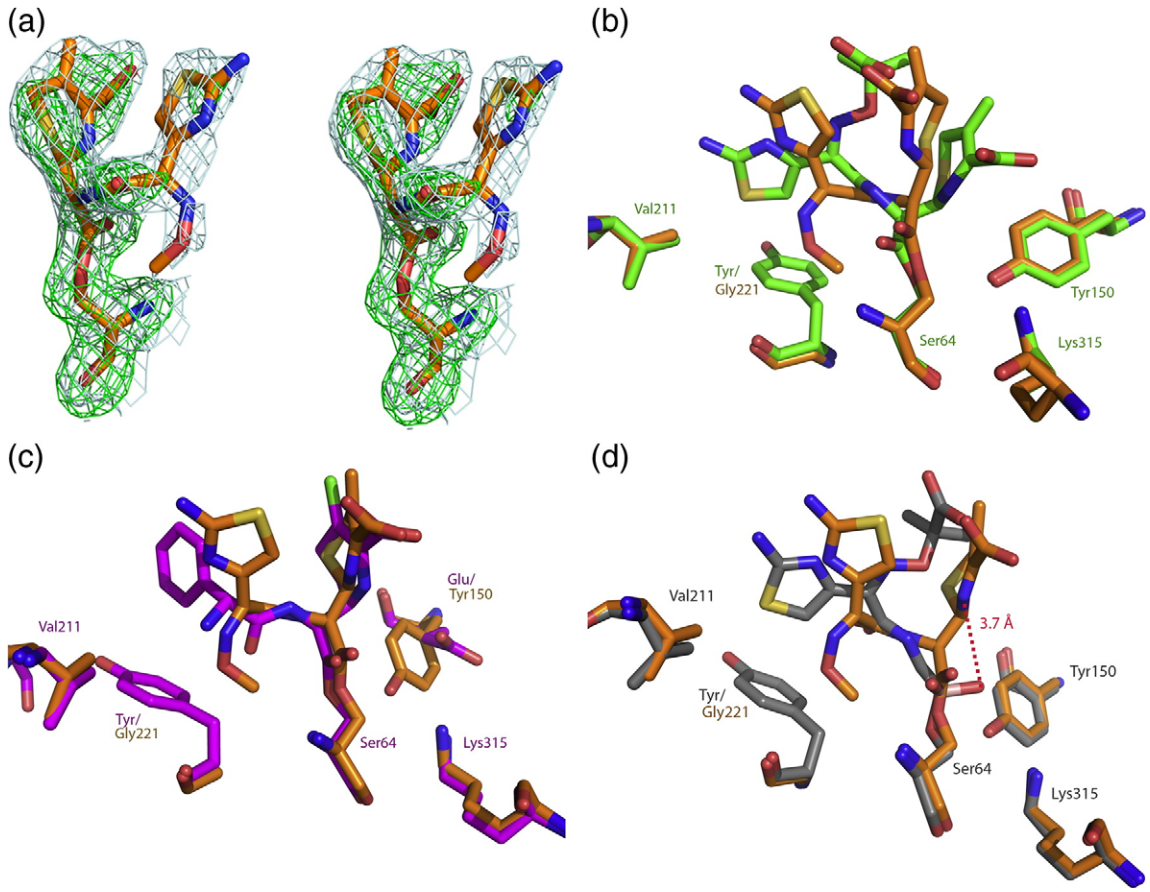

Fig. 7. X-ray structure of Y221G/cefotaxime (2.3 Å). (a) Stereo view of the quality of cefotaxime density in the active site of Y221G. $2F_o - F_c$ density (blue) is shown at a contour level of 1σ, and $F_o - F_c$ omit density (green) is shown at a contour level of 3σ. (b) The Y221G/cefotaxime structure (orange) overlaid with the WT/ceftazidime structure (green). (c) The Y221G/cefotaxime structure (orange) overlaid with the WT/loracarbef structure (purple). (d) The Y221G/cefotaxime structure (orange) overlaid with the WT/ceftazidime deacylation transition-state analog (gray).

of Tyr221 to a glycine creates a cavity, which alleviates the steric clash that occurs with the catalytically competent conformation of the third-generation cephalosporins (see the text below). This opens up space in the active site that is only partially filled by Asp217, adopting a new conformation and moving into its place.

Y221G/cefotaxime structure

Y221G crystals were soaked in a solution of 1.7 M KPi (pH 8.7) and 50 mM cefotaxime for 1 h and then flash frozen to obtain a structure of the Y221G/cefotaxime complex. The structure of the Y221G/cefotaxime complex was determined by X-ray crystallography to 2.3 Å resolution (R_{work} = 19.6%, R_{free} = 24.8%; Table 2). Strong $2F_o - F_c$ electron density was seen for the ligand at 1σ in the B monomer and in an $F_o - F_c$ omit map at 3σ (Fig. 7a). We compared the Y221G/cefotaxime structure to the crystal structure of WT AmpC in complex with the closely related third-generation cephalosporin ceftazidime (Fig. 7b).[31] Cefotaxime, which for the Y221G mutant enzyme has become a good substrate, adopts a conformation different from that adopted by ceftazidime in its complex with WT AmpC (Fig. 7b), where the third-generation cephalosporin is such a poor substrate that it functions as a covalent inhibitor. The new conformation of cefotaxime in the active site of Y221G resembles that of good substrates, such as loracarbef, in WT AmpC[49] (Fig. 7c). Cefotaxime's adoption of the loracarbef-like structure in the Y221G complex appears to make it competent for catalysis. In contrast with the AmpC/ceftazidime structure, where the lactam nitrogen of substrate is only 1.8 Å from where the attacking water is expected to be in the deacylation high-energy intermediate, this same nitrogen has moved 3.7 Å from the putative water position in the Y221G/cefotaxime structure, making it competent for catalysis (Fig. 7d).[31] This movement is, in turn, allowed by the introduction of the cavity in Y221G, increasing the volume of the active site and its ability to accommodate third-generation cephalosporins.

Discussion

Two key observations emerge from this study. First, each of the five mutant enzymes has achieved its 2-order-of-magnitude activity gains at the cost of substantial stability loss. The minimum stability loss is 1.7 kcal mol^{-1} (3.3 °C) for T70I, whereas V298E loses 4.1 kcal mol^{-1} (7.4 °C), fully 30% of the net stability of the native protein. Second, the crystal structures reveal that the substitutions, although distant from one another by up to 30 Å, have the same overall effect, enlarging the active site by introducing physical defects and allowing the mutant enzymes to accommodate the large third-generation cephalosporins. We consider these points in turn.

Destabilization of mutant enzymes

The stability insults conferred by these gain-of-function substitutions are easily appreciated. In V298E, substituting a charged residue into a well-packed hydrophobic core causes a cascade of conformational changes that are revealed in the X-ray structure of the mutant enzyme (Fig. 4). Similarly, in Y221G, the substitution introduces a straightforward structural defect, creating a hole in the protein structure and loss of van der Waals interactions that are only partially fulfilled by the movement of Asp217 into this region. In the H210AAA insertion mutant, the expanded Ω-loop conformation reduces packing, van der Waals interactions, hydrogen bonding, and hydrophobic surface area burial (Fig. 5). Finally, both T70I and E219K lose hydrogen bonds that ordinarily stabilize this same Ω-loop region of the enzyme. In WT AmpC, the hydroxyl of Thr70 hydrogen bonds with the backbone carbonyl of Glu219 in this loop, while this interaction has been lost and not replaced in the structure of T70I, leading to substantial conformational change in the mutant protein (Fig. 6). In E219K, the substitution of the lysine disrupts a hydrogen bond that, in the WT enzyme, the native glutamate side chain made to its own backbone nitrogen, which otherwise has no partner in the WT structure. This internal hydrogen bond stabilizes the loop conformation adopted in this region of the structure, and its loss is likely responsible for the destabilization of E219K. Thus, all five mutant enzymes are textbook illustrations of how to disrupt protein structure and stability, should that ever be one's goal.

Translating stability loss into activity gain

The activity that these mutants need to gain is the ability to hydrolyze β-lactam substrates that are too large for the native active site, the third-generation cephalosporins. Each of the mutants accomplishes this by introducing structural insults to the integrity of the protein. Three mechanisms may be considered through which these stability defects are translated into increased activity: by changing the ground state of the enzyme, by changing enzyme flexibility, or by changing its dynamics. Here, we will not further distinguish between flexibility and dynamics, as our structural and thermodynamic results are insufficiently resolved to do so, but we will simply refer to both under the rubric of "flexibility," understanding that dynamics may play a role.

Perhaps the simplest mutant to understand is Y221G, which changes the ground-state apo conformation of the enzyme to accommodate third-generation cephalosporins. Tyr221 is a highly conserved residue whose presence forces third-generation cephalosporins into a catalytically incompetent conformation, owing to a steric clash with their large R1 side chains (see the text above). Substitution of Tyr221 with a glycine allows the β-lactam to relax into a catalytically competent

conformation. Thus, in the Y221G/cefotaxime complex (Fig. 7), this third-generation cephalosporin adopts a conformation resembling that adopted by good substrates in WT X-ray structures (Fig. 7c). Similarly, the X-ray structure of H210AAA reveals a well-resolved larger conformation for the Ω-loop, indicating a change in the ground state for this mutant enzyme. This insertion effectively replaces Val211 with an alanine; Val211 is the second residue, in addition to Tyr221, that clashes with the R1 side chain of third-generation cephalosporins in WT AmpC. This structure is largely consistent with that of the enzyme inspiring our work on this mutant, the clinically isolated GC1 ESBL from *E. cloacae*.[32–34,47] One difference between the two structures is that the GC1 apo structure revealed local disorder in residues 213–215,[32] including one residue of the insertion, suggesting increased flexibility relative to that of the P99 enzyme. Conversely, in the AmpC apo structure, the Ω-loop adopts a new well-ordered conformation that expands active-site volume (Fig. 5).

The V298E mutant falls into the same category of affecting the ground-state conformation of the enzyme—enlarging it—although flexibility may also play a role here. The introduction of a glutamate into the hydrophobic core of the protein is a gross structural insult; to relieve this, the enzyme undergoes substantial reorganization, flipping the now Glu298 into bulk solvent. This perturbation (21 Å from the catalytic serine) begins a cascade of structural changes, starting with a flip of Trp260 into the hole created by the movement of Glu298. What used to be the loop defined by residues 285–296, which in the WT structure formed a bounding wall of the active site, is both moved outwards and disordered (it has largely disappeared from the electron density maps), reflecting both increased active-site volume and, potentially, flexibility. The net effect is to increase the volume of the active site, improving its ability to accommodate the catalytically competent conformation of the bulky third-generation cephalosporins. This then provides a relatively rare structural view into a phenomenon that is common to resistance enzymes as diverse as dihydrofolate reductase,[42] human immunodeficiency virus (HIV) protease,[40] HIV reverse transcriptase,[50] and BCR-ABL kinase[41]—the occurrence of resistance substitutions far from the active site.

The mutant enzymes T70I and E219K appear to gain activity against third-generation cephalosporins via increased flexibility. The T70I apo structure has two notable conformational changes relative to WT: notwithstanding the 2.14-Å resolution to which it was determined, density is missing for residues 193–221 in the active-site "Ω-loop," and an active-site β-turn (residues 318–322) has flipped conformations to disrupt the catalytically critical oxyanion hole, formed by the backbone nitrogens of Ser64 and Ala318. Since this mutant enzyme is catalytically active, the X-ray structure can only represent one conformation that is accessible to the protein, suggesting that it is more flexible. Indeed, in the complex with the transition-state analog BZB, the active site of T70I resolves into a conformation that is again catalytically competent, resembling the native active site in conformation and overall volume. These observations are consistent with activity being gained by increased flexibility in T70I, which appears to be much more plastic on ligand binding than does the WT enzyme.[51] The situation with E219K is more subtle. We observe little substantial conformational change in either the E219K apo structure or the inhibitor-bound structure relative to WT AmpC, although the mutant is 150-fold more active against cefotaxime. The loss of the internal hydrogen bond between the side chain and the backbone nitrogen of residue 219 appears to loosen the structure, with the 215–216 peptide bond adopting a second conformation in the holo structure, while residues 211–213 also undergo a conformational change (Fig. 6d). Neither of these conformations is seen in a 1.07-Å structure of WT AmpC[52] that revealed other inherent conformational states, suggesting increased flexibility in the E219K enzyme, again in the Ω-loop region.

How do these results fit with the stability–activity tradeoff model? At the simplest level, the observation that the AmpC ESBLs have, in every case, lost stability is consistent with the model. At atomic resolution, too, the structural underpinnings of the "stability–function" hypothesis are confirmed—larger, more difficult substrates are recognized by the introduction of stability defects that increase either the ground-state size of the AmpC active site or its ability to flex when confronted by the larger substrates.

It is this physical basis of the model that is the key to understanding where the "stability–function" hypothesis is relevant and how it may be reconciled with the observations of other groups. Clearly, stability–activity tradeoffs are not linked by physical law; one can imagine substitutions that increase stability without an effect on activity—indeed, the stability-restoring mutant in TEM-1 ESBLs, M182T, is an example of such,[20,22] and the evolution of thermophilic mutants that do not sacrifice activity is another.[24] Nor does the evolution of new function necessarily require stability sacrifices. Indeed, results from this study suggest that an enzyme could mutate to a new substrate profile and *gain* stability. Thus, for all five mutant enzymes studied here, the k_{cat} values for smaller first-generation substrates such as cephalothin are actually *reduced* typically by 3-fold to 8-fold, and by 100-fold for Y221G for the destabilized mutants (Table 1). The same increase in active-site volume and flexibility that allows the larger third-generation cephalosporins to be accommodated by the AmpC ESBL mutants decreases complementarity for smaller substrates, which fit the native active site snugly. If one inverts the evolution of AmpC and imagines that Y221G is the native enzyme, then one would be able to evolve a "mutant" that has the WT sequence with 100-fold *greater* activity for the smaller

cephalothin and has substantially improved stability. This would be a case where the active site has shrunk and new interactions with the rest of the folded protein have been (re)introduced, consistent with the physical model underlying the "stability–function" hypothesis.

Still, this case remains the exception that proves the rule. In enzymes evolving under the pressure of antimicrobial or antineoplastic chemotherapy, such as dihydrofolate reductase,[42] HIV protease,[40] BCR-ABL tyrosine kinase,[41] HIV reverse transcriptase,[50] and β-lactamases, gain-of-function mutants and many inhibitor-resistant mutants are likely to sacrifice stability, not because stability is a necessary correlate to activity, by some implied law, but because introduction of structural defects or further preorganization into active sites typically reduces stability. It is a testament to the importance of stability in enzyme evolution that "restabilizing" and "recatalyzing" substitutions have been found *in vivo* to compensate for activity and stability losses occurring as side effects of primary drug resistance substitutions.[20–22,53] The role of stability as a constraint in enzyme evolution[23,27] may well have implications for strategies to reduce resistance evolution under chemotherapeutic pressure.[27]

Materials and Methods

Construction and purification of AmpC β-lactamases

Mutants of AmpC were created using the overlap extension polymerase chain reaction.[54] Both WT and mutant enzymes were expressed and purified as described,[49,55] except for Y221G, where the cells were lyzed using a Microfluidizer M-110 at 18,000 psi in 50 mM Tris–HCl (pH 7) and the lysate was purified. The mutant enzymes were purified from an *m*-aminophenylboronic acid affinity column.[55]

Kinetic measurements

The activity of each mutant enzyme was determined by its hydrolysis of the β-lactam substrate cephalothin (Sigma, St. Louis, MO) in a 50 mM Tris–HCl buffer containing 0.01% Triton X (pH 7.0). Reaction rates were measured with a Hewlett-Packard HP-8453 spectrometer. k_{cat} and K_m values were determined from Michaelis–Menten plots, and parameters were fitted using Kaleidagraph (Synergy, Reading, PA). The extinction coefficients used were as follows: AmpC, 2.45 OD mg^{-1} ml^{-1} cm^{-1}; cephalothin, $\Delta\varepsilon_{265} = -8790$ M^{-1} cm^{-1}; cefotaxime, $\Delta\varepsilon_{260} = -6710$ M^{-1} cm^{-1}. At high substrate concentrations, 1-mm pathlength cuvettes were used to obtain kinetic data.

Crystallization and structure determination

AmpC extended-spectrum mutants were crystallized under the following conditions: V298E: 30% polyethylene glycol 8000, 0.1 M sodium cacodylate, and 0.2 M ammonium sulfate (pH 6.5); Ω-loop insertion: 1.7 M KPi (pH 8.0); T70I/BZB and E219K/BZB: 1.7 M KPi (pH 8.7) and 360 μM BZB; Y221G and E219K: 1.7 M KPi (pH 8.7). Y221G was also soaked in 50 mM cefotaxime and 1.7 M KPi (pH 8.7) for 1 h. Diffraction was measured at beamline 8.3.1 of the Advanced Light Source (Lawrence Berkeley National Laboratories, Berkeley, CA). Reflections were indexed, integrated, and scaled using MOSFLM[56] and SCALA in CCP4.[57] Molecular replacement was accomplished with MOLREP in CCP4,[57] using the appropriate apo structure, typically the WT structure [Protein Data Bank (PDB) ID 1KE4], as search model. Model building and refinement were completed with Coot[58] and REFMAC5[59] in the CCP4 suite.[57]

Thermal denaturation

Enzymes were denatured by raising the temperature in 0.1 °C increments at a ramp rate of 2 °C min^{-1} in 50 mM potassium phosphate (pH 6.8), 50 mM potassium chloride, and 38% (vol/vol) ethylene glycol buffer, using a Jasco 715 spectropolarimeter with a Peltier effect temperature controller and an in-cell temperature monitor.[46] Denaturation was marked by an obvious transition in the far-UV CD (223 nm) signal. Consistent with previous work with AmpC enzymes, which demonstrated a reversible two-state behavior (see Results),[10,46] all mutant enzyme melts were reversible and apparently two-state, as judged by >90% return of CD signal upon quick cooling following denaturation and a clear, sharp transition in the denaturation curve. Denaturation of two representative mutant enzymes (Y221G and H210AAA) was also measured by the intensity of the integrated fluorescence emission for all wavelengths above 300 nm, exciting at 280 nm, using a fluorescence detector on the Jasco instrument, and was compared to thermal denaturation monitored by far-UV CD to investigate two-state behavior. Temperature of melting (T_m) and van't Hoff enthalpy of unfolding (ΔH_{vh}) values were calculated using EXAM.[60] The free energy of unfolding relative to WT was calculated using the method of Becktel and Schellman: $\Delta\Delta G_u = \Delta T_m \Delta S_u^{WT}$.[61] A negative value of $\Delta\Delta G_u$ indicates stability loss. The ΔS_u^{WT} was 0.56 kcal mol^{-1} K^{-1}.[46]

PDB accession codes

X-ray crystal structure coordinates have been deposited in the PDB with the following accession codes: V298E (PDB ID 3IXD), H210AAA (PDB ID 3IWI), T70I/BZB (PDB ID 3IXG), Y221G (PDB ID 3IWO), Y221G/CTX (PDB ID 3IXH), E219K (PDB ID 3IWQ), and E219K/BZB (PDB ID 3IXB).

Acknowledgements

This work was supported by National Institutes of Health grant GM63813 (to B.K.S.). V.L.T. was partly supported by a National Science Foundation Predoctoral Fellowship. We thank Sandri Soelaiman and Ray Nagatani for mutagenesis, protein purification, and set-up of crystal trays; Kerim Babaoglu, Yu Chen, and Pascal Egea for crystallographic assistance; Christian Laggner for advice and assistance with chemical intuition, Matthew Merski for molecular biology assistance, and Sarah Boyce and Jens Carlsson for a review of this manuscript.

Supplementary Data

Supplementary data associated with this article can be found, in the online version, at doi:10.1016/j.jmb.2009.11.005

References

1. Warshel, A. (1978). Energetics of enzyme catalysis. *Proc. Natl Acad. Sci. USA*, **75**, 5250–5254.
2. Warshel, A., Sussman, F. & Hwang, J. -K. (1988). Evaluation of catalytic free energies in genetically modified proteins. *J. Mol. Biol.* **201**, 139–159.
3. Herzberg, O. & Moult, J. (1991). Analysis of the steric strain in the polypeptide backbone of protein molecules. *Proteins*, **11**, 223–229.
4. Clackson, T. & Wells, J. A. (1995). A hot spot of binding energy in a hormone–receptor interface. *Science*, **267**, 383–386.
5. Richards, F. M. (1974). The interpretation of protein structures: total volume, group volume distributions and packing density. *J. Mol. Biol.* **82**, 1–14.
6. Williams, R. J. (1972). The entatic state. *Cold Spring Harbor Symp. Quant. Biol.* **36**, 53–62.
7. Meiering, E. M., Serrano, L. & Fersht, A. R. (1992). Effect of active site residues in barnase on activity and stability. *J. Mol. Biol.* **225**, 585–589.
8. Schreiber, G., Buckle, A. M. & Fersht, A. R. (1994). Stability and function: two constraints in the evolution of barstar and other proteins. *Structure*, **2**, 945–951.
9. Shoichet, B. K., Baase, W. A., Kuroki, R. & Matthews, B. W. (1995). A relationship between protein stability and protein function. *Proc. Natl Acad. Sci USA*, **92**, 452–456.
10. Beadle, B. M. & Shoichet, B. K. (2002). Structural bases of stability–function trade-offs in enzymes. *J. Mol. Biol.* **321**, 285–296.
11. Ota, M., Isogai, Y. & Nishikawa, K. (1997). Structural requirement of highly-conserved residues in globins. *FEBS Lett.* **415**, 129–133.
12. Mukaiyama, A., Haruki, M., Ota, M., Koga, Y., Takano, K. & Kanaya, S. (2006). A hyperthermophilic protein acquires function at the cost of stability. *Biochemistry*, **45**, 12673–12679.
13. Hargrove, M. S. & Olson, J. S. (1996). The stability of holomyoglobin is determined by heme affinity. *Biochemistry*, **35**, 11310–11318.
14. Chen, Y. C. & Lim, C. (2008). Common physical basis of macromolecule-binding sites in proteins. *Nucleic Acids Res.* **36**, 7078–7087.
15. Liang, S., Zhang, J., Zhang, S. & Guo, H. (2004). Prediction of the interaction site on the surface of an isolated protein structure by analysis of side chain energy scores. *Proteins*, **57**, 548–557.
16. Ota, M., Kinoshita, K. & Nishikawa, K. (2003). Prediction of catalytic residues in enzymes based on known tertiary structure, stability profile, and sequence conservation. *J. Mol. Biol.* **327**, 1053–1064.
17. Kidokoro, S., Miki, Y., Endo, K., Wada, A., Nagao, H., Miyake, T. *et al.* (1995). Remarkable activity enhancement of thermolysin mutants. *FEBS Lett.* **367**, 73–76.
18. Zhi, W., Srere, P. A. & Evans, C. T. (1991). Conformational stability of pig citrate synthase and some active-site mutants. *Biochemistry*, **30**, 9281–9286.
19. Garcia, C., Nishimura, C., Cavagnero, S., Dyson, H. J. & Wright, P. E. (2000). Changes in the apomyoglobin folding pathway caused by mutation of the distal histidine residue. *Biochemistry*, **39**, 11227–11237.
20. Wang, X., Minasov, G. & Shoichet, B. K. (2002). Evolution of an antibiotic resistance enzyme constrained by stability and activity trade-offs. *J. Mol. Biol.* **320**, 85–95.
21. Huang, W. & Palzkill, T. (1997). A natural polymorphism in beta-lactamase is a global suppressor. *Proc. Natl Acad. Sci. USA*, **94**, 8801–8806.
22. Sideraki, V., Huang, W., Palzkill, T. & Gilbert, H. F. (2001). A secondary drug resistance mutation of TEM-1 beta-lactamase that suppresses misfolding and aggregation. *Proc. Natl Acad. Sci. USA*, **98**, 283–288.
23. Weinreich, D. M., Delaney, N. F., Depristo, M. A. & Hartl, D. L. (2006). Darwinian evolution can follow only very few mutational paths to fitter proteins. *Science*, **312**, 111–114.
24. Giver, L., Gershenson, A., Freskgard, P. O. & Arnold, F. H. (1998). Directed evolution of a thermostable esterase. *Proc. Natl Acad. Sci. USA*, **95**, 12809–12813.
25. Bloom, J. D., Labthavikul, S. T., Otey, C. R. & Arnold, F. H. (2006). Protein stability promotes evolvability. *Proc. Natl Acad. Sci. USA*, **103**, 5869–5874.
26. Bloom, J. D. & Arnold, F. H. (2009). In the light of directed evolution: pathways of adaptive protein evolution. *Proc. Natl Acad. Sci. USA*, **106**, 9995–10000.
27. Tokuriki, N. & Tawfik, D. S. (2009). Chaperonin overexpression promotes genetic variation and enzyme evolution. *Nature*, **459**, 668–673.
28. Massova, I. & Mobashery, S. (1998). Kinship and diversification of bacterial penicillin-binding proteins and beta-lactamases. *Antimicrob. Agents Chem.* **42**, 1–17.
29. Galleni, M., Lamotte-Brassear, J., Raquet, X., Dubus, A., Monnaie, D., Knox, J. R. & Frere, J. -M. (1995). The enigmatic catalytic mechanism of active-site serine beta-lactamases. *Biochem. Pharmacol.* **49**, 1171–1178.
30. Matagne, A., Misselyn-Bauduin, A. M., Joris, B., Erpicum, T., Granier, B. & Frere, J. M. (1990). The diversity of the catalytic properties of class A beta-lactamases. *Biochem. J.* **265**, 131–146.
31. Powers, R. A., Caselli, E., Focia, P. J., Prati, F. & Shoichet, B. K. (2001). Structures of ceftazidime and its transition-state analogue in complex with AmpC beta-lactamase: implications for resistance mutations and inhibitor design. *Biochemistry*, **40**, 9207–9214.
32. Crichlow, G. V., Kuzin, A. P., Nukaga, M., Mayama, K., Sawai, T. & Knox, J. R. (1999). Structure of the extended-spectrum class C beta-lactamase of *Enterobacter cloacae* GC1, a natural mutant with a tandem tripeptide insertion. *Biochemistry*, **38**, 10256–10261.
33. Nukaga, M., Kumar, S., Nukaga, K., Pratt, R. F. & Knox, J. R. (2004). Hydrolysis of third-generation cephalosporins by class C beta-lactamases. Structures of a transition state analog of cefotoxamine in wild-type and extended spectrum enzymes. *J. Biol. Chem.* **279**, 9344–9352.
34. Nukaga, M., Taniguchi, K., Washio, Y. & Sawai, T. (1998). Effect of an amino acid insertion into the omega loop region of a class C beta-lactamase on its substrate specificity. *Biochemistry*, **37**, 10461–10468.
35. Matsumura, N., Minami, S. & Mitsuhashi, S. (1998). Sequences of homologous beta-lactamases from clinical isolates of *Serratia marcescens* with different substrate specificities. *Antimicrob. Agents Chemother.* **42**, 176–179.
36. Raimondi, A., Sisto, F. & Nikaido, H. (2001). Mutation in *Serratia marcescens* AmpC beta-lactamase produc-

ing high-level resistance to ceftazidime and cefpirome. *Antimicrob. Agents Chemother.* **45**, 2331–2339.
37. Zhang, Z., Yu, Y., Musser, J. M. & Palzkill, T. (2001). Amino acid sequence determinants of extended spectrum cephalosporin hydrolysis by the class C P99 beta-lactamase. *J. Biol. Chem.* **276**, 46568–46574.
38. Tsukamoto, K., Ohno, R., Nukaga, M. & Sawai, T. (1992). The effect of amino acid substitution at position 219 of *Citrobacter freundii* cephalosporinase on extension of its substrate spectrum. *Eur. J. Biochem.* **207**, 1123–1127.
39. Morosini, M. I., Negri, M. C., Shoichet, B., Baquero, M. R., Baquero, F. & Blazquez, J. (1998). An extended-spectrum AmpC-type beta-lactamase obtained by *in vitro* antibiotic selection. *FEMS Microbiol. Lett.* **165**, 85–90.
40. Muzammil, S., Ross, P. & Freire, E. (2003). A major role for a set of non-active site mutations in the development of HIV-1 protease drug resistance. *Biochemistry*, **42**, 631–638.
41. Shah, N. P., Nicoll, J. M., Nagar, B., Gorre, M. E., Paquette, R. L., Kuriyan, J. & Sawyers, C. L. (2002). Multiple BCR–ABL kinase domain mutations confer polyclonal resistance to the tyrosine kinase inhibitor imatinib (STI571) in chronic phase and blast crisis chronic myeloid leukemia. *Cancer Cell*, **2**, 117–125.
42. Volpato, J. P. & Pelletier, J. N. (2009). Mutational 'hotspots' in mammalian, bacterial and protozoal dihydrofolate reductases associated with antifolate resistance: sequence and structural comparison. *Drug Resist. Updates*, **12**, 28–41.
43. Dubus, A., Wilkin, J. M., Raquet, X., Normark, S. & Frere, J. M. (1994). Catalytic mechanism of active-site serine beta-lactamases: role of the conserved hydroxy group of the Lys-Thr(Ser)-Gly triad. *Biochem. J.* **301**, 485–494.
44. Trehan, I., Morandi, F., Blaszczak, L. C. & Shoichet, B. K. (2002). Using steric hindrance to design new inhibitors of class C beta-lactamases. *Chem. Biol.* **9**, 971–980.
45. Mazzella, L. J. & Pratt, R. F. (1989). Effect of the 3′-leaving group on turnover of cephem antibiotics by a class C beta-lactamase. *Biochem. J.* **259**, 255–260.
46. Beadle, B. M., McGovern, S. L., Patera, A. & Shoichet, B. K. (1999). Functional analyses of AmpC beta-lactamase through differential stability. *Protein Sci.* **8**, 1816–1824.
47. Nukaga, M., Haruta, S., Tanimoto, K., Kogure, K., Taniguchi, K., Tamaki, M. & Sawai, T. (1995). Molecular evolution of a class C beta-lactamase extending its substrate specificity. *J. Biol. Chem.* **270**, 5729–5735.
48. Powers, R. A., Blazquez, J., Weston, G. S., Morosini, M. I., Baquero, F. & Shoichet, B. K. (1999). The complexed structure and antimicrobial activity of a non-beta-lactam inhibitor of AmpC beta-lactamase. *Protein Sci.* **8**, 2330–2337.
49. Patera, A., Blaszczak, L. C. & Shoichet, B. K. (2000). Crystal structures of substrate and inhibitor complexes with AmpC-lactamase: possible implications for substrate-assisted catalysis. *J. Am. Chem. Soc.* **122**, 10504–10512.
50. Ghosn, J., Chaix, M. L. & Delaugerre, C. (2009). HIV-1 resistance to first- and second-generation non-nucleoside reverse transcriptase inhibitors. *AIDS Rev.* **11**, 165–173.
51. Beadle, B. M., Trehan, I., Focia, P. & Shoichet, B. K. (2002). Structural milestones in the pathway of an amide hydrolase: substrate, acyl, and product complexes of cephalothin with AmpC β-lactamase. *Structure*, **10**, 413–424.
52. Chen, Y., Minasov, G., Roth, T. A., Prati, F. & Shoichet, B. K. (2006). The deacylation mechanism of AmpC beta-lactamase at ultrahigh resolution. *J. Am. Chem. Soc.* **128**, 2970–2976.
53. Schock, H. B., Garsky, V. M. & Kuo, L. C. (1996). Mutational anatomy of an HIV-1 protease variant conferring cross-resistance to protease inhibitors in clinical trials. Compensatory modulations of binding and activity.. *J. Biol. Chem.* **271**, 31957–31963.
54. Ho, S. N., Hunt, H. D., Horton, R. M., Pullen, J. K. & Pease, L. R. (1989). Site-directed mutagenesis by overlap extension using the polymerase chain reaction. *Gene*, **77**, 51–59.
55. Usher, K. C., Blaszczak, L. C., Weston, G. S., Shoichet, B. K. & Remington, S. J. (1998). Three-dimensional structure of AmpC beta-lactamase from *Escherichia coli* bound to a transition-state analogue: possible implications for the oxyanion hypothesis and for inhibitor design. *Biochemistry*, **37**, 16082–16092.
56. Leslie, A. G. W. (1992). Recent changes to the MOSFLM package for processing film and image plate data. *Jt. CCP4+ESF-EAMCB Newsl. Protein Crystallogr.*, 26.
57. Collaborative Computational Project, No. 4. (1994). The CCP4 suite: programs for protein crystallography. *Acta Crystallogr. Sect. D*, **50**, 760–763.
58. Emsley, P. & Cowtan, K. (2004). Coot: model-building tools for molecular graphics. *Acta Crystallogr. Sect. D*, **60**, 2126–2132.
59. Murshudov, G. N., Vagin, A. A. & Dodson, E. J. (1997). Refinement of macromolecular structures by the maximum-likelihood method. *Acta Crystallogr. Sect. D*, **53**, 240–255.
60. Kirchoff, W. (1993). *EXAM: A Two-State Thermodynamic Analysis Program*. NIST Publication, Gaithersburg, MD.
61. Becktel, W. J. & Schellman, J. A. (1987). Protein stability curves. *Biopolymers*, **26**, 1859–1877.